Journal of Asian Earth Sciences: X 12 (2024) 100183

Contents lists available at ScienceDirect

Journal of Asian Earth Sciences: X

journal homepage: www.sciencedirect.com/journal/journal-of-asian-earth-sciences-x

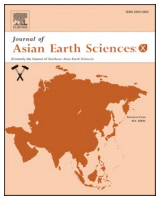

Anthropogenic impacts on the water chemistry of a transboundary river system in Southeast Asia

Duc A. Trinh [a,*], Nga T. Do [a,b], Virginia N. Panizzo [c], Suzanne McGowan [d], Jorge Salgado [e], Andy R.G. Large [f], Andrew C.G. Henderson [f], Thuy T. Vu [g]

[a] Nuclear Training Center, Vietnam Atomic Energy Institute, 140 Nguyen Tuan, Thanh Xuan, Ha Noi, Viet Nam
[b] Electric Power University, 235 Hoang Quoc Viet, Bac Tu Liem, Ha Noi, Viet Nam
[c] Centre for Environmental Geochemistry, School of Geography, University of Nottingham, University Park, Nottingham NG7 2RD, United Kingdom
[d] Department of Aquatic Ecology, Netherlands Institute of Ecology, Droevendaalsesteeg 10, 6708PB Wageningen, the Netherlands
[e] Department of Geography, University College London, United Kingdom
[f] School of Geography, Politics and Sociology, Newcastle University, Newcastle Upon Tyne NE1 7RU, United Kingdom
[g] Faculty of Engineering and Science, Curtin University, CDT 250, 98009 Miri Sarawak, Malaysia

ARTICLE INFO

Keywords:
Major ions
Acidification
Urbanization
Agriculture
Red River

ABSTRACT

The Red River originating from Yunnan province, China is the second largest river in Vietnam in terms of length and discharge. Combination of water chemistry monitoring data of 4 years (2018–2022) from different sub-basins of the Red River (the Da, Lo, Thao, Tra Ly, and Day) with historical datasets indicates a decline in pH from 8.1 in 2000 to 7.7 in 2021, greater CO_2 concentrations and a shift from waters naturally dominated by carbonate weathering to waters dominated by evaporite weathering. Such changes were most apparent in the delta area where heavy human activities have increased influxes of most dissolved chemicals, except SiO_2. Evaporite weathering is particularly enhanced by mining and deforestation occurring in upstream regions of both China and Vietnam. Pyrite oxidation, alongside silicate weathering, is enhanced along the Red River Fault Zone but reduced in tributaries with a higher proportion of hydropower reservoirs. Longer water residence times in these large reservoirs (total volume $> 2.7x10^{10}$ m^3) located in the Da and Lo sub-basins have also increased primary productivity, leading to higher evasion/uptake of CO_2 and SiO_2, lower total dissolved solids (TDS), and higher pH. The total physical and chemical denudation rates of upstream mountain tributaries ranged between 0.107 ± 0.108 and 0.139 ± 0.137 mm yr^{-1}, mainly due to reservoir implementation and instream aquatic biogeochemistry changes. Our findings demonstrate that anthropogenic activities are profound factors impacting the water chemistry of the Red River system.

1. Introduction

The processes of physical and chemical weathering are the primary natural mechanisms by which solutes and particulate materials are released into rivers, and in general the combination of evaporite dissolution and pyrite oxidation, silicate weathering, and carbonate weathering are the major determinants of river water chemistry. Anthropogenic activities, including mining for aggregates and minerals, urban expansion and associated increases in industrial and domestic pollution, and the intensification of agriculture which increases runoff from fertilizers and other agrochemicals have also been altering river water chemistry (Chen et al., 2003). Anthropogenic impacts are changing riverine CO_2 and pH, for example through eutrophication and increased inputs of organic matter (Salgado et al., 2022). As conduits and biogeochemical reactors of organic matter (Ward et al., 2017), rivers which receive large quantities of organic carbon have elevated partial pressures of CO_2 (pCO_2) and lower pH (Drake et al., 2017; Ward et al., 2017). Consequently, urbanization can increase the potential for rivers to be emit CO_2 (Xiao et al., 2017). Another important influence on the pH of river waters is mining which can promote soil acidification, lower water pH and increase the runoff of particulates (Guo et al., 2015; Yang et al., 2014). Pollution-related acidification of precipitation from fossil fuel burning can also influence river water chemistry through the direct addition of ions (SO_4^{2-}, NO_3^-), but acidification effects on waters are

* Corresponding author.
E-mail addresses: trinhanhduc@yahoo.com, trinhanhduc@vinatom.gov.vn (D.A. Trinh).

https://doi.org/10.1016/j.jaesx.2024.100183
Received 25 April 2024; Received in revised form 21 July 2024; Accepted 12 August 2024
Available online 14 August 2024

highly modified by geology and soils. The pH of surface waters influences the availability of dissolved silica but anthropogenic activities can have positive or negative effects on silica (Kubo et al., 2022; Michel, 1987; van Dokkum et al., 2004). Engineering modifications to the configuration of rivers is occurring in many systems and such physical alterations have the potential to influence water chemistry. For example, impoundments through damming are increasingly common in economically-developing tropical regions of Southeast Asia (Nguyen et al., 2021; Roberts et al., 2022 McGowan et al., 2023). Reservoirs create sinks that act as traps for certain elements such as calcite and silica (Maavara et al., 2014). The channelization of rivers in urban areas of intensive water withdrawal and use creates increasingly lentic or stagnant conditions which, in combination with high pollution loads, increases ionic concentrations in river waters and strengthens the potential for river CO_2 outgassing (Xiao et al., 2017; Yang et al., 2014). Irrigation for agriculture also alters the hydrological pathways for the exchange of solutes among terrestrial and aquatic environments (Duc et al., 2020). Each of these processes interacts with natural weathering to determine the composition of solutes in river waters.

Most long-term studies of changes in river water chemistry have taken place in north temperate climate zones where rivers have been significantly impacted by intensive human activities over a longer period of time (Renwick, 1991). These studies (Meybeck, 2002) reported that there have been notable increases in riverine Na^+, Cl^-, and SO_4^{2-} (ions characteristic of evaporite weathering) since the 1960 s, while the concentrations of Ca^{2+}, Mg^{2+}, and HCO_3^- (ions associated with carbonate weathering) have remained stable (Weiler & Chawla, 1969; Berner, 1971; Renwick, 1991; Vitaly et al., 1998). For rivers in tropic climate, it is also expected that the human alteration to river water chemistry, both scale and tendency, is recently significant. In fact, tropical rivers play a significant role in the hydrogeochemical cycling of elements by transporting continental weathered and anthropogenic products to the oceans (Nisha et al., 2022; Stallard, 1988). Despite covering only 25 % of the Earth's land surface, tropical rivers are responsible for delivering 38 % of the ocean's dissolved ions (Sharma et al., 2022), 65 % of dissolved silica (Michel, 1987) and up to 64 % of C (Li et al., 2017). There have been reports of the water quality and hydrology changes due to our present actions in rivers locating in economic-developing, tropical regions such as in the highly populated regions of Southeast Asia (Nguyen et al., 2021; Roberts et al., 2022; McGowan et al., 2023). Still, we see the gaps in our understanding of progressive anthropogenic impacts to river water chemistry, resulting in drastic changes of such pH, dissolved CO_2, dissolved SiO_2, and water facies.

Located in a sub-tropical area of rapid economic development, the Red River Basin (RRB) in China and Vietnam provides an ideal setting to study chemical weathering under natural and human altered conditions. This river (named Hong He in China), is among the world's 60 largest ranked by dissolved load (Gaillardet et al., 1999) and is an unstable fluvial system in which the geographical configuration has been extensively altered by both natural and human-induced processes (Li, 2016). For this transboundary river basin, ecological, environmental and geological degradation has increased markedly both in Yunnan province (China) and northern Vietnam. For example, from 2010 to 2022 Yunnan province in China lost 63.8 kha of humid primary forest, making up 6.6 % of its total tree cover loss in the same time period (Global Forest Watch, 2024). Consequently, the upper RRB has been identified as a dry-hot valley area with forest areas being completely stripped away below 1200 m above sea level, leaving only barren mountains and "unruly" waters (Li, 2016). The river system has also been subjected to the implementation of multiple cascading hydropower dams (Nguyen et al., 2021) and a rapid rise in population density with associated urbanization over the last two decades (Luu et al., 2021).

The Red River water chemistry has rarely been investigated. Moon et al. (2007) concluded that anthropogenic factors were trivial controls of water chemistry in the upstream mountain area and did not study long-term trends in weathering in this river system, comparing only two sampling times (2002–2003). At this time, Vietnam and China, were less developed and since then there has been no systematic, long-term monitoring programme of the water chemistry of this river system. To fill this gap, we combined water chemistry data from two major monitoring programmes on the Red River – the NERC-NAFOSTED programme and the UKRI-GCRF Living Deltas Hub- which both provided 48 consecutive months of data across the RRB in Vietnam from March 2018 – February 2022. Our aim was to assess recent anthropogenic impacts on river water chemistry, including the effects of: river impoundments on dissolved and suspended solid trapping; ion enrichment from carbonate and evaporite weathering; mining and industrialization on water acidification; and agriculture and urbanization on the carbon load and river CO_2 enrichment. Particular efforts were made to assess the SiO_2 and CO_2 variabilities in sub-basins that are heavily impounded and urbanized, to address recent global concerns that impacted rivers are increasingly becoming CO_2 sources and SiO_2 depleted (Maavara et al., 2014). While these impacts on river water chemistry have been widely reported elsewhere, they have never been fully addressed in the Red River system. We also re-assessed weathering rates and the composition of dominant elements across the different sub-basins and calculated the current RRB denudation rates.

2. Materials and methods

2.1. Study area

The Red River originates in the southeastern part of the Tibetan Plateau in Yunnan Province, China and flows along the NW–SE trending Red River Fault Zone (RRFZ) to the Gulf of Tonkin in the Vietnam East Sea (Fig. 1a). The headwaters of the Thao are composed of thick Upper Triassic to Lower Cenozoic sequences of coal-bearing continental clastic rocks (Burchfiel & Wang, 2003; Leloup et al., 1995; Wang et al., 2005). Mafic and ultramafic intrusions hosting sulfide deposits are also exposed along the RRFZ (Wang et al., 2005). The Da sub-basin is covered with Paleozoic and Mesozoic continental red beds, close to the RRFZ, Permo-Carboniferous limestones (Leloup et al., 1995). Felsic and ultramafic rocks are limited to a few scattered exposures near the RRFZ. The Lo sub-basin is characterized by a thick marine succession of Triassic limestone and fine-grained clastic rocks (Burchfiel & Wang, 2003). Between the Lo main channel and its largest tributary, the Chay River, Vietnam, Proterozoic to Lower Paleozoic low-grade metamorphic and sedimentary rocks are exposed along with small granitoid intrusions (Wysocka & Swierczewska, 2003). The geological structure of the uppermost part of the Red River delta (RRD) consists of a continuous layer of Pleistocene gravel overlain by islands of Pleistocene sand and clay. The Pleistocene deposits are covered by a thick layer of fine-grained floodplain and deltaic deposits that were exposed to alluvial erosion at the southwest margin of the floodplain and along the recent Red River course and replaced by coarse grained channel belt deposits and fine-grained floodplain and oxbow lake deposits.

A marked difference in rainy/dry and summer/winter seasons characterize the region. In the RRD region, the rainy season starts (lasts until) May (November) and peaks in August and September. The hottest month is June and the coldest is January (Supporting information Figure S1). The offset in timing between rainy/dry and summer/winter seasonality can lead to a time difference between biogeochemical activities and dilution/erosion effects.

While the upstream river network is distinctively separated into 3 sub-basins (Da, Lo, and Thao), the river network in the delta is very dense and heavily modified for irrigation and drainage purposes with almost 3 % of the land area being covered by rivers and irrigation canals (Joern et al., 2024) (Fig. 1b). The main rivers flowing through the RRD region include the Red River, Tra Ly River, and Day River (Luu et al., 2021). Mean discharge from the Day River is 1848 km^3/yr (Luu et al., 2010). The RRD has a diurnal tidal regime which ranges from 2.6 to 3.6

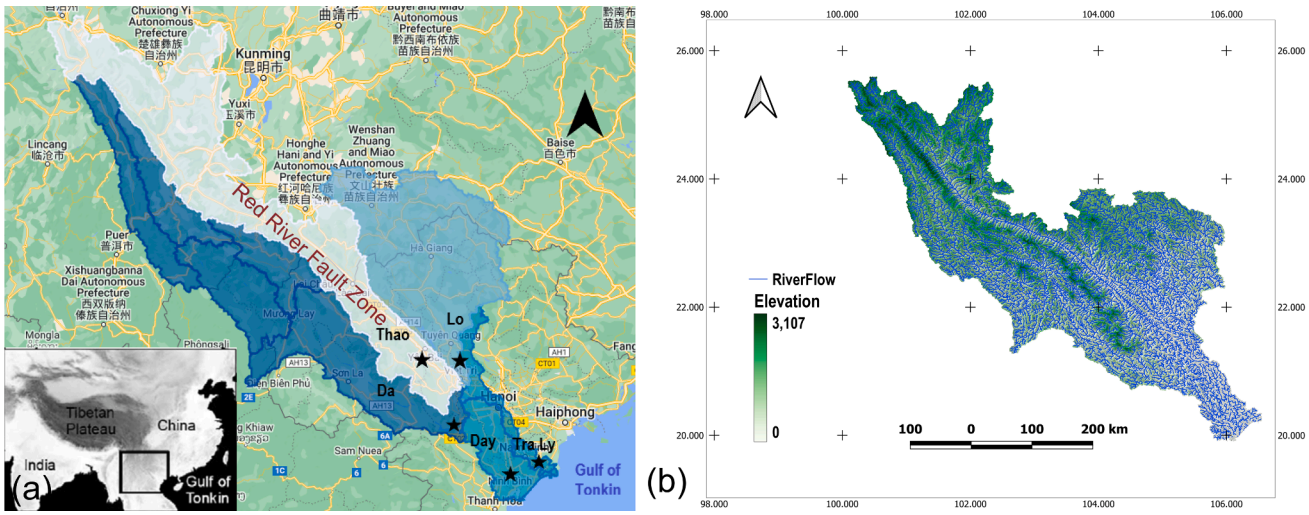

Fig. 1. (a) Three upstream mountainous sub basins: the Da, Thao, and Lo and two downstream delta sub basins: the Day and Tra Ly. Stars indicate the monitoring sites. (b) the river network of the Red River Basin.

m as recorded at a hydrological monitoring station, around 50 km NE of the mouth of the Red River (NCMH, 2017).

2.2. Water sampling and chemical analysis and secondary data collection

Based on the river hydrology, a set of monitoring sites (location names in parentheses; Table 1) within the territory of Vietnam was established to include tributaries in the mountainous areas, namely the Thao (Yen Bai), Lo (Vu Quang), and Da (Hoa Binh) Rivers, and in the delta, the Day (Gian Khau) and Tra Ly River (Quyet Chien). Water was sampled monthly from March 2018 to February 2022 but no sampling took place in August and September 2021 due to the global Covid-19 pandemic. Physico-chemical parameters (pH, total dissolved solids [TDS]) were measured in-situ by a Hydrolab sonde DS5. Each sample was analyzed in the laboratory for major cations (Ca^{2+}, Mg^{2+}, Na^{+}, and K^{+}), major anions (Cl^{-}, SO_4^{2-} and HCO_3^{-}) and dissolved silica (SiO_2).

The cations Na^{+} and K^{+} were analyzed by flame-AAS according to SMEWW 3500 in Clesceri et al., (1998) with detection limits of 0.1 mg/L for both Na^{+} and K^{+}, respectively. Titration with ethylenediaminetetraacetic acid (EDTA) was used to analyze total hardness and Ca EDTA hardness with a detection limit of 2 mg/L (0.05 mmol/L). Mg^{2+} was calculated from total hardness minus Ca EDTA. Concentrations of Cl^{-} were determined using silver nitrate (0.02 mmol/L) titration with chromate indicator (Mohr's method) according to the SMWW 3500 K – C method from (Clesceri et al., 1998). Alkalinity (HCO_3^{-}) was determined by titration with HCl 0.1 mol/L and a bromocresol blue-methyl red indicator according to the SMWW 2320 method from (Clesceri et al., 1998). In circumneutral waters, OH^{-} is about 4 orders of magnitude smaller than HCO_3^{-}, thus alkalinity ($[OH^{-} + HCO_3^{-}]$) is basically equal to HCO_3^{-}. The SMWW 4500SO_4-E gravimetric method (Clesceri, et al., 1998) was used to analyze SO_4^{2-} in water. An acidic media with $BaCl_2$ was used to form homogeneous $BaSO_4$ and the resulting suspension was measured using a UV–Vis spectrophotometer at a wavelength of 490 nm. The SMWW 4500SiO_2 C molybdosilicate method (Clesceri et al., 1998) was used to determine SiO_2 in water samples by adding ammonium molybdate at pH~1.2 to form heteropoly acid from silica and measuring the yellow color on a UV–VIS spectrophotometer at a wavelength of 410 nm. Daily discharge and total suspended solid (TSS) contents at the sampling sites were collected by the Vietnam Meteorology and Hydrology Administration.

2.3. Denudation rate calculation

Here we define the denudation rate as the total delivery of terrestrial dissolved and solid materials into the river. The denudation rate is the sum of the chemical denudation rate (i.e. the amount of total dissolved solids; TDS) and the physical denudation rate (the amount of total suspended solids; TSS) in the water.

Total dissolved solids (TDS):

$$TDS\left(mass \bullet volume^{-1}\right) = \sum anions + \sum cations$$

TDS yield:

$$TDSyield\left(mass \bullet area^{-1} time^{-1}\right) = \frac{TDS\left(mass \bullet volume^{-1}\right) \bullet Discharge\left(volume \bullet time^{-1}\right)}{Surfacearea(area)}$$

Chemical denudation rate:

$$Chemicaldenudationrate\left(length \bullet time^{-1}\right) = \frac{TDSyield\left(mass \bullet area^{-1} volume^{-1}\right)}{Density\left(mass \bullet volume^{-1}\right)}$$

Physical denudation rate:

$$Physicaldenudationrate\left(length \bullet time^{-1}\right) = \frac{TSSyield\left(mass \bullet area^{-1} volume^{-1}\right)}{Density\left(mass \bullet volume^{-1}\right)}$$

2.4. Carbonate – Evaporite – Silicate end member ternary plot

To assess silicate weathering in relation to carbonate and evaporite processes and hence the relative importance of gypsum versus pyrite between the different catchments, we applied $HCO_3^{-} - SiO_2 - [Cl^{-} + SO_4^{2-}]$

ternary diagrams (Moon, et al., 2007) to determine the dominant weathering processes in relation to silicate weathering as follows:

Gypsum dissolution generates data near the ($Cl^- + SO_4^{2-}$) apex because it produces SO_4^{2-}, not silicate and carbonate;

Pyrite oxidation and accompanying carbonate weathering generates data along the Alk – [$Cl^- + SO_4^{2-}$] axis because it produces SO_4^{2-} and HCO_3^-, not silicate. Additionally, anthropogenic inputs may contribute SO_4^{2-}, Cl^-, and HCO_3^- but not SiO_2. In many cases, SiO_2 is taken up by primary producers as an essential nutrient at a faster pace than weathering and SiO_2 is lost;

Pyrite oxidation accompanied by silicate weathering generates data toward the center of the ternary diagram because sulfuric acid generates high sulfate, neutralizes the HCO_3^-, and dissolves silicates;

Calcite and dolomite dissolution generate data near the Alk apex because it produces alkalinity.

2.5. Calcite saturation index (CSI) and excess carbon dioxide partial pressure ($EpCO_2$) calculations

To calculate the excess carbon dioxide partial pressure ($EpCO_2$) in the river waters, the following equation derived from (Trinh, et al., 2009) was used:

$$EpCO_2 = \frac{Alk.10^{6-pH}}{11.7}$$

Where Alk. is alkalinity (μmol/L).

The calcite saturation index (CSI) is calculated as:

$CSI = \log([Ca^{2+}] \cdot [CO_3^{2-}]/K_{calcite})$.

Where $K_{calcite}$ is the saturation coefficient of calcite.

3. Results

3.1. Water chemistry at sub-basin level

Violin plots unmistakably reveal that the majority of ions are enriched in the western bank delta section (Day River) (Fig. 2), which is also the most densely populated area in the Red River Basin (Luu et al., 2021). However, SiO_2, and HCO_3^- exhibit distinct variations, suggesting that they are influenced by additional factors such as sediment–water-atmosphere exchanges or instream biological activities. To test for significant differences between the sub-basin water chemistry, paired t-tests were applied to the few datasets which were normally distributed, but otherwise the nonparametric pair sample signed test was then used (for Na^+, K^+, Ca^{2+}, Mg^{2+}, SiO_2, Cl^-, SO_4^{2-}, and HCO_3^-). The results show a similarity in water chemistry between the Da and Lo sub-basins and a difference of the Day sub-basin water chemistry from other sub-basins.

The Gibbs diagram (supporting information figure S2) suggests that the rock-water interaction controls the upstream water chemistry (Thao, Lo, Da), while mixing of upstream waters (Tra Ly) with domestic and industrial wastewater inflows (Day), indicated by increases of TDS, Na, and Cl, gradually modified the water chemistry in the downstream catchments. In the dry season when river flows from upstream are feeble, anthropogenic impacts became more visible, and data points plots towards evaporation dominance in the Gibbs plot.

3.2. Seasonality of water chemistry

The two types of seasonality: dry and rainy (December – May and June – November), and summer and winter (April – September and October – March) (supporting information Figure S1) determine temperature, irradiance, and hydrology (rainfall, discharge) in the rivers. Consequently, these climatic variations significantly influence weathering processes, elemental dilution, the magnitude of anthropogenic impact, and river biogeochemical processes (Duc et al., 2007). Across different tributaries, TDS and major ions are mainly higher during the dry than the rainy season (Fig. 3). Variables such as Mg^{2+}, Ca^{2+}, and HCO_3show a more pronounced rainy-dry seasonality compared to Na^+, K^+, Cl^-, or SO_4^{2-} (Table 2). Conversely, the variability of SiO_2 demonstrates a stronger correlation with the summer – winter seasonality than the rainy – dry seasonality at certain sites (Fig. 3a, h, Table 2). In particular, pH shows significant variation within both seasonality categories.

Piper plots generated from the mean values for the dry (December – May) and rainy (June – November) seasons helped to distinguish seasonal differences (Supporting information Figure S3) and indicate that throughout both seasons, the RRB is predominantly characterized by the [Ca^{2+}-Mg^{2+}–HCO_3^-] type/facies. Among all sites, the Day River site exhibits the least (the most) [Ca^{2+}-Mg^{2+}–HCO_3^-] ([Na^+-K^+-Cl^-]) facies, a pattern which was accentuated during the dry season (Supporting information Figure S3). Overall, the dominant [Ca^{2+}-Mg^{2+}–HCO_3^-] facies identified in the Piper plots aligns with findings from previous studies on the Red River water chemistry (Luu et al., 2021; Moon et al., 2007).

4. Discussion

4.1. Anthropogenic impacts on the RRB reflected in the spatial–temporal variability of water chemistry

4.1.1. Decadal

Since the economic reforms of the late 1970 s in China and the late 1980 s in Vietnam, the RRB has experienced a major socioeconomic transformation, leading to widespread landscape alterations and environmental degradation (Duc et al., 2007; Trinh et al., 2012). Our understanding of how this transformation has influenced river water chemistry is limited, but our findings indicate that over the past two decades, there has been a gradual shift in water chemistry. For instance, pH recorded during our monitoring period averaged 7.7 ± 0.4 with a range of 6.6 to 8.6 (Fig. 2a, 3a), comparable to the range reported by (Hoang et al., 2020) for the same sites in 2019 (range = 6.9 – 7.4) but half a pH point lower than the mildly alkaline (mean = 8.1) values reported by Moon et al. (2007) for the upstream region in 2001–2002 and by (Le et al., 2018) for the downstream region in 2014 (mean = 8.1). This declining pH tendency concurs with measurements from other similarly river systems which have been anthropogenically impacted in the Tibetan plateau (Guo et al., 2015). Concurrently, there is a systematic change of lithologies over time, from carbonates toward evaporites in the RRB (Fig. 4).

The alignment of the sample poles parallel to the trend between silicate/evaporite and carbonate weathering domains, implies possible mixing between silicate/evaporite and carbonate end members (Fig. 4). Among the three upstream tributaries, the Lo is more carbonate-enriched while the Thao tends towards silicate/evaporite, in agreement with the work of Moon et al. (2007). In the RRD region, the Day tributary is close to the global centroid while the Tra Ly tributary is close to the center of the upstream tributaries. However, in contrast with previous work of Moon et al. (2007), our results show a notable shift in the Red River water chemistry since the 2020s, moving closer towards the global level, indicating a growing dominance of evaporite (Cl^-, K^+, Na^+) than in the 2000s. Moreover, water chemistry in the urbanized delta section (Day River) has a greater dominance of evaporite ions (SO_4^{2-}, Cl^-) compared to the other sub-basins (Fig. 4). The recent shift

Table 1
Location of the sampling sites.

Station name	River reach	Longitude (°E)	Latitude (°N)	Altitude (m)
Yen Bai	Thao River	104.88333	21.70000	60
Vu Quang	Lo River	105.25000	21.56667	22
Hoa Binh	Da River	105.31667	20.81667	120
Gian Khau	Day River	105.91667	20.31667	3
Quyet Chien	Tra Ly River	106.2000	20.5000	3

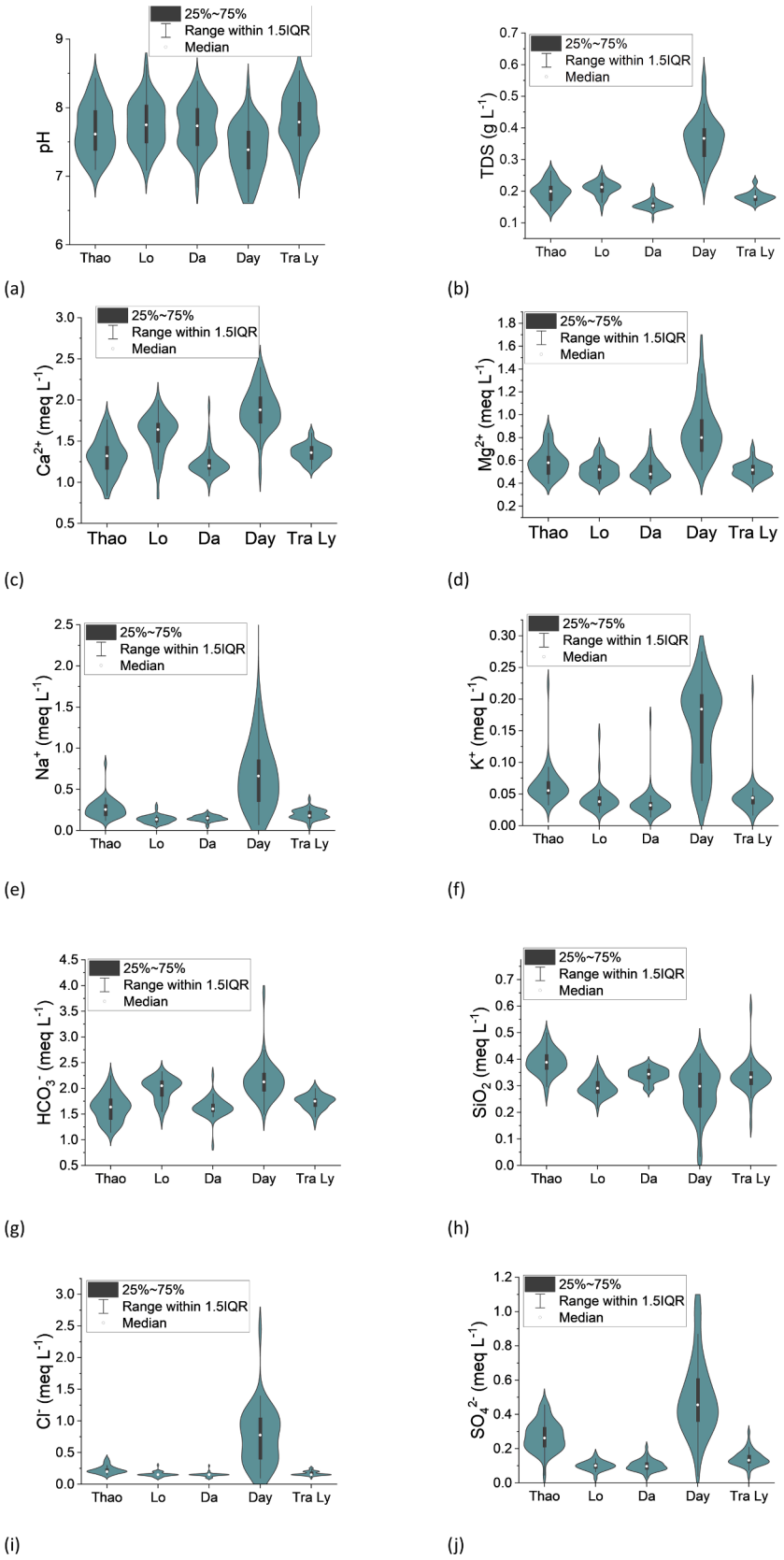

Fig. 2. Violin plots of water chemistry data (pH, TDS, and 8 major ions) at different sub-basins collected between March 2018 and February 2022. The plots show distinctive water chemistry of the Day sub-basin where anthropogenic activities occur most and different patterns of water chemistry among upstream mountain sub-basins – Thao, Lo, and Da.

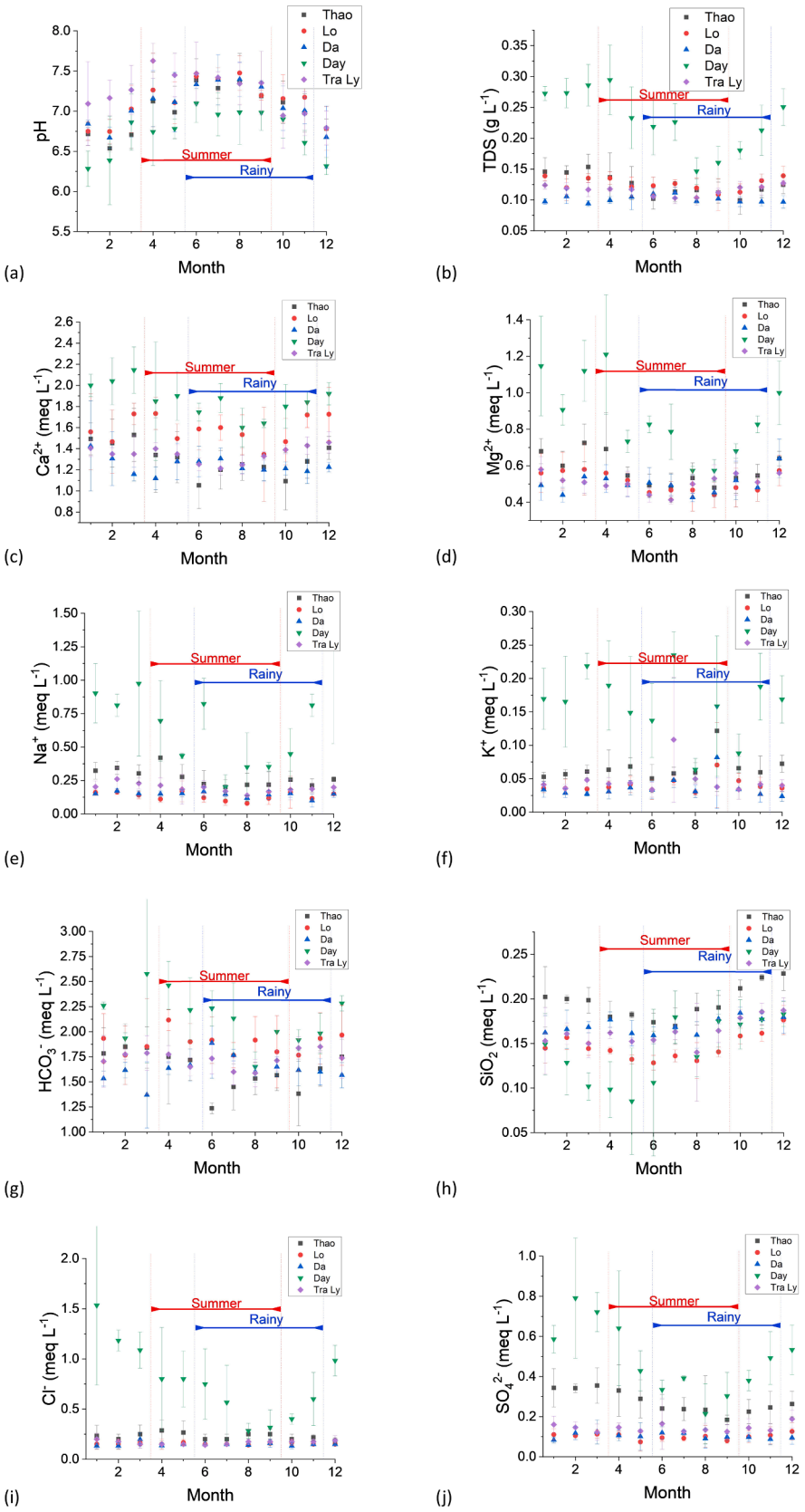

Fig. 3. Monthly average of water chemistry (mean ± SD) of Thao, Lo, and Da upstream tributaries, and Day and Tra Ly delta tributaries show clearly 2 patterns of seasonal variabilities; the summer – winter seasonality represented by such pH and SiO_2 and the rainy – dry seasonality represented by such TDS, Na^+, Mg^{2+}, HCO_3^-, Cl^-, SO_4^{2-}.

Table 2
Two sample *t*-test values for dry – rainy (winter – summer) seasons. Bold: significant difference at 0.05 level.

Site	pH	TDS	Na^+	K^+	Ca^{2+}	Mg^{2+}	SiO_2	HCO_3^-	Cl^-	SO_4^{2-}
Thao	**$2.7e^{-5}$ ($3.1E^{-3}$)**	**$1.1E^{-4}$**	0.12	0.42	**$7.8E^{-4}$**	**$1.2E^{-5}$**	0.38 (**$4.3E^{-7}$**)	**$1.1E^{-4}$** (0.07)	0.37	**$1.9E^{-3}$**
Lo	**$6.5E^{-5}$ ($1.8E^{-3}$)**	**$9.0E^{-3}$**	0.16	0.56	0.20	**$1.7E^{-4}$**	0.78 (**$1.2E^{-4}$**)	0.28 (0.56)	0.14	0.15
Da	**$1.0E^{-4}$ ($2.8E^{-3}$)**	0.13	0.31	0.09	0.77	0.20	0.99 (**0.05**)	0.06 (**0.01**)	0.65	0.99
Day	**$3.3E^{-3}$ ($3.9E^{-3}$)**	**$3.0E^{-7}$**	**$6.5E^{-4}$**	0.11	**$5.2E^{-3}$**	**$1.6E^{-5}$**	**0.02** (0.18)	**$8.5E^{-3}$** (0.07)	**$3.1E^{-5}$**	**$1.9E^{-5}$**
Tra Ly	**$6.3E^{-5}$ ($3.0E^{-3}$)**	**$2.5E^{-4}$**	0.08	0.32	**$1.7E^{-3}$**	**$4.4E^{-3}$**	0.39 (**$2.4E^{-2}$**)	**$1.5E^{-2}$** (0.76)	**$4.6E^{-2}$**	0.36

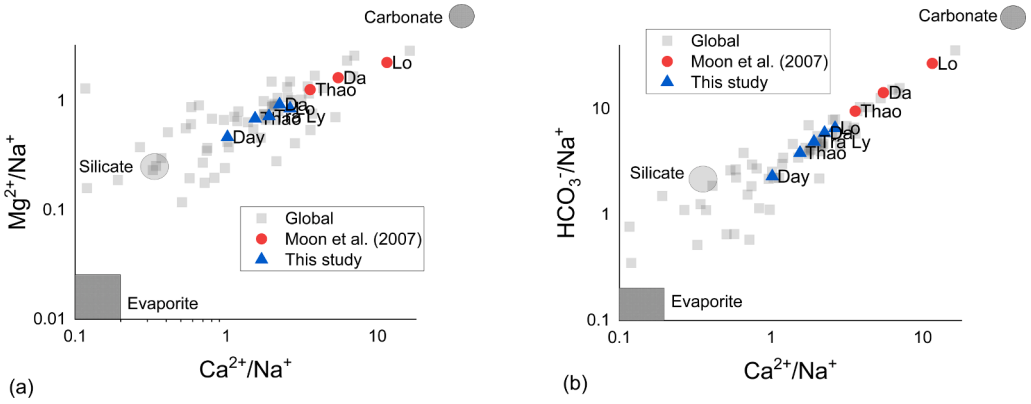

Fig. 4. (a) The Na^+ −normalized Mg^{2+} versus Na^+ −normalized Ca^{2+} plot and (b) The Na^+ −normalized HCO_3^- versus Na^+ −normalized Ca^{2+} plot after (Gaillardet, et al., 1999; Moon, et al., 2007). Endmembers of Evaporites: $Ca^{2+}/Na^+ \approx 0.2$, $Mg^{2+}/Na^+ \approx 0.025$, and $HCO_3^-/Na^+ \approx 0.2$; Silicates: $Ca^{2+}/Na^+ = 0.35 \pm 0.15$, $Mg^{2+}/Na^+ = 0.24 \pm 0.12$, and $HCO_3^-/Na^+ = 2 \pm 1$; and Carbonates: $Ca^{2+}/Na^+ \approx 50$, $Mg^{2+}/Na^+ \approx 10$, and $HCO_3^-/Na^+ \approx 120$.

towards a water chemistry dominated by evaporite weathering in the RRD region, fits well with the observed decline in pH and the heightened anthropogenic impacts in the river basin. We hypothesize that these systematic decadal-scale trends from alkaline towards circumneutral pH and from carbonate towards evaporite could be attributed to both climate changes and anthropogenic activities. Extreme climate events such as intense rainfall and heatwaves can increase weathering, carbonate distribution, clay illuviation, organic matter decomposition, and acidification (Scharpenseel & Becker-Heidmann, 1990; Varallyay, 2010). Additionally, anthropogenic activities including deforestation, reservoir building, mining, acid rain, and urbanization contribute to increased acidity in soil and water (Galloway, 2001). The progressive acidification of water is concerning for its potential impacts on ecosystem functioning, since calcareous aquatic species like molluscs may become extinct at pH<6.5 (Claudi et al., 2012). Also, many freshwater species cannot tolerate to water enriched with Cl^- and SO_4^{2-} (Moore et al., 2019). Furthermore, at the sites with low pH and enriched SO_4^{2-} and Cl^-. dissolved oxygen was usually low, further indicating a link with human impacts and organic matter pollution. Such oxygen stress can have further deleterious effects on ecosystem functioning (Dos Reis Oliveira et al., 2019).

4.1.2. Spatial

Water chemistry surveys from 2001 to 2002 concluded that anthropogenic inputs of dissolved substances was minimal in the upstream Da, Lo, and Thao tributaries (Moon et al., 2007). However, our long-term monitoring of water chemistry indicates that recent anthropogenic activities (river damming, mining, and urban expansion) are increasingly impacting water chemistry in both the downstream delta and the upstream tributaries. Hydropower dams/river impoundments increase water residence time, which creates lentic and less physically disturbed conditions for the development of phytoplankton primary producers. The increases in photosynthesis and growth consumes SiO_2 and CO_2, to lower SiO_2 and increase pH as observed in Da and Lo Rivers where hydropower dams are concentrated (Nguyen et al., 2021). Mining activities, particularly pyrite oxidation of sulfide deposit exhumation, results in low pH and elevated concentrations of Na^+, K^+, SiO_2 and SO_4^{2-} in the Thao sub-basin (Yang et al., 2014). Urbanization contributes to organic matter pollution and biological oxygen demand through untreated sewage inputs and the associated CO_2 production during decomposition reduces pH and leads to enrichment of all major ions except SiO_2 (Duong et al., 2019; Salgado et al., 2022). Accordingly, ranking of SiO_2 concentrations and pH across the sub-basins in our study was Thao > Da > Lo (see next sub-section), compared with Thao < Da and < Lo in Moon et al. (2007). The reversal in our data can likely be attributed to the expansion of large hydropower reservoirs across the Da and Lo Rivers since the 2000 s. These reservoirs have a cumulative volume > $1.4x10^{10}$ m^3 (Nguyen et al., 2021), forming large standing waters where SiO_2 is utilized by siliceous algae (diatoms) and sequestered into reservoir sediments, lowering the SiO_2 concentrations and increasing the pH in the Da and Lo river waters relative to the Thao (Fig. 2h, 3 h). The resulting heightened primary productivity also contributes to elevated pH levels (refer to Fig. 2a, 3a). Simultaneously, the burgeoning mining industry for gold, tin, zinc, copper, iron, and coal along the RRFZ, situated within the Thao tributary (Liu et al., 2021; Yang et al., 2014) may further augment the solute inputs (K^+, Na^+, Cl^-, SiO_2, and SO_4^{2-}) into the waters relative to the other two upstream sub-basins. It is well-understood that the oxidation of spoil materials from mining activities, containing S, P, and N bearing minerals, results in the formation of acidic ions SO_4^{2-}, PO_4^{3-}, NO_3^- upon exposure. Consequently, this process lowers pH and increases the dissolution of cations. Moreover, the processing and pre-treatment of mined ores often involve the use of strongly alkaline or acidic solutions and it is possible that these chemicals contribute solutes to river waters.

4.1.3. Seasonal

The seasonal variation between summer and winter influences primary production (Duong et al., 2019), and with it the uptake and release of certain solutes such as SiO_2 and HCO_3^-. Primary productivity involves the assimilation of HCO_3^- and H^+ from water to form organic matter (most simply CH_2O) and produces dissolved oxygen (O_2). This process typically increases pH in surface water whereas respiration and biological degradation consume oxygen and produce CO_2. In neutral water, CO_2 forms HCO_3^- and produces H^+, leading to a reduction of pH (Duc

et al., 2009). Primary production by diatoms involves SiO_2 uptake, resulting in a SiO_2 seasonality related to the degree of primary productivity (Duong et al., 2019). The rainy-dry seasonality also influences physical weathering and dilution of numerous solutes. This seasonality is most pronounced in the Day River where most solutes are significantly higher during the dry season relative to the rainy season (Table 2). The Day River receives two main water sources: natural water derived from rainfall, characterized by diluted major ions, and the polluted water from urban and industrial areas, characterized by concentrated major ions (Roberts et al., 2022). As rainfall increases between dry and rainy seasons, the Day River water chemistry fluctuates seasonally accordingly. However, the seasonal patterns differ in other, less urbanized tributaries of the RRB. For instance, the Thao sub-basin presents a rainy-dry seasonal signal for some ions, except the alkaline ions and Cl^-. In the Lo sub-basins, only Mg^{2+} varies between the rainy-dry seasons, while in the Da sub-basin, no major ion exhibits seasonal variations. The Tra Ly River indicates a mixture of upstream sub-basin characteristics and some anthropogenic inputs, with half of the major ions (Ca^{2+}, Mg^{2+}, HCO_3^-, and Cl^-) showing a significant rainy-dry seasonal signal. Notably, in all three upstream sub-basins, SiO_2 varies significantly between winter and summer (Table 2), indicating a biogeochemical influence on the seasonality.

The inconsistent seasonal variability among major ions was reported by Moon et al. (2007) who suggested that the upstream tributaries did not undergo simple dilution in dissolved chemical concentrations with increasing water discharge. As discussed above, we suspect that the main anthropogenic impacts in the upstream tributaries might be mining rather than domestic waste as seen in the urbanized tributary. Not all major ions are concentrated due to such impacts. For instance, some major ions (e.g., Na^+, SO_4^{2-}) sourced from certain activities like mining might experience a dilution effect, while other ions (e.g., Cl^-) deriving from processes such as acid rain or natural dissolution might not. The dry-rainy seasonality of Cl^- was indistinct in the upstream sub-basins ($prob>|t| > 0.05$) (Da, Thao, and Lo) implying evaporite dissolution or acid rain as the main contributor, but it was significantly seasonal in the delta area ($prob>|t| < 0.05$) (Day and Tra Ly), indicating urban sources as the main contributor. There was limited evidence of SO_4^{2-} dry-rainy seasonality in the Da, Lo, and Tra Ly sub-basins ($prob>|t| > 0.05$), which could be attributed to the effects of damming and/or insignificant pyrite oxidation (as see later). In contrast, significant SO_4^{2-} dry-rainy seasonality ($prob>|t| < 0.05$) implies pyrite oxidation in the Thao sub-basin and urban impact in the Day sub-basin. In the Da, Lo, Thao and Tra Ly tributaries, the SiO_2 rainy-dry seasonality is weaker than the SiO_2 summer-winter seasonality, indicating that biological activity plays an important role and there is higher uptake of SiO_2 in the summer than the winter. However, in the Day tributary, the significant dry-rainy SiO_2 seasonality implies that urbanization is a major influential factor. The HCO_3^- dry-rainy seasonality is significant ($prob>|t| < 0.05$) in the Thao, Tra Ly, and Day Rivers (Table 2). However, the variability of HCO_3^- can be attributed to multiple factors including instream primary production/respiration and sediment–water-atmospheric exchanges. We observe significantly lower $[HCO_3^-]$ in the dry season than the rainy season and in winter than in summer in the Da River, indicating that instream biological activities are important controls on $[HCO_3^-]$ in this tributary. Together with the fact that the Da River stream flow is highly altered by numerous large hydropower dams, it is challenging to assess which specific anthropogenic impacts contribute to the $[HCO_3^-]$ seasonality.

In summary, our analysis leads us to conclude that selected major ions in the upstream tributaries are predominantly derived from anthropogenic activities, with mining activities likely being the primary contributor and concentrated mostly in the Thao tributary. This conclusion is further supported by the assessment of solute concentrations. For instance, SO_4^{2-}, an inert anion produced by weathering, acid rain, and probably anthropogenic inputs, exhibits similar concentrations to regional rainwater (40 μmol/L; EANET, 2021) in the Da and Lo but is nearly 3 times higher in the Thao tributary. Silica, associated with the SO_4^{2-} production, experiences a dilution effect. Chloride levels throughout the Red River are approximately 10 times higher than regional rainwater, underscoring the importance of evaporite weathering (as discussed later), which experiences no dilution effect. Bicarbonate is produced/consumed by various processes, including carbonate weathering (which follows a rainy-dry charge/dilution effect), atmospheric/sediment exchange (unaffected by rainy-dry or summer-winter variation), and biological processes (which fluctuate with summer-winter seasonality).

4.2. Evaporite dissolution, pyrite oxidation, silicate weathering, and carbonate productivity

Evaporite deposits consist predominantly of minerals formed through the evaporation of saline solutions. Geologically, the Red River is aligned with the Red River Fault, which extends for approximately 1000 km from the southeast corner of the Tibetan Plateau to the Gulf of Tonkin (Fig. 1). Along the Red River Fault, metamorphic complexes have been exhumed and are covered in many parts by carbonate rock formation, spanning an area of 50,000 km^2 in northern Vietnam (Drogue et al., 2000). Carbonate rocks such as calcite/aragonite ($CaCO_3$) and dolomite ($CaMg(CO_3)_2$), halite (NaCl) and gypsum ($CaSO_4{\cdot}2H_2O$)/anhydrite ($CaSO_4$) are the most common evaporites that can affect river water composition. A notable characteristic of evaporite dissolution is that it produces equivalent/balanced charges between major cations and anions. Weathering processes involving other chemicals may introduce an imbalance in the charge. In light of this characteristic, we first examine the charge balance between alkaline cations and Cl^- (Fig. 5) to identify the processes governing alkalinity and $[Cl^-]$ in the water.

As most subsets were not normally distributed, we applied nonparametric paired sample sign tests to assess if charge balance (the indifference between $[Na^+ + K^+]$ and Cl^-) in each tributary. Our analyses revealed that $[Na^+{+}K^+]$ is statistically balanced with Cl^- in the Lo and Day tributaries whereas $[Na^+{+}K^+]$ exceeds Cl^- in the Thao, Da, and Tra Ly tributaries. Specifically, in the Thao, Da, and Tra Ly tributaries, Cl^- concentrations were significantly lower than $[Na^+{+}K^+]$, indicating the addition of Na^+ and K^+ from other weathering and/or anthropogenic processes. Moon et al. (2007) suggested pyrite oxidation accompanied by Na/K-silicate weathering occurring in the Thao and the Da are processes that release additional alkaline cations into the rivers. Mining activities along the RRFZ may also contribute to the enrichment of Na^+, K^+, and Cl^- in the Thao River. In the Lo tributary, the equality between Cl^- and $[Na^+ + K^+]$, indicates that dissolution of halite, and to a lesser extent sylvite, dominates the weathering of Na^+, K^+, and Cl^-. The water in the Tra Ly tributary is mainly mixed from three upstream waters

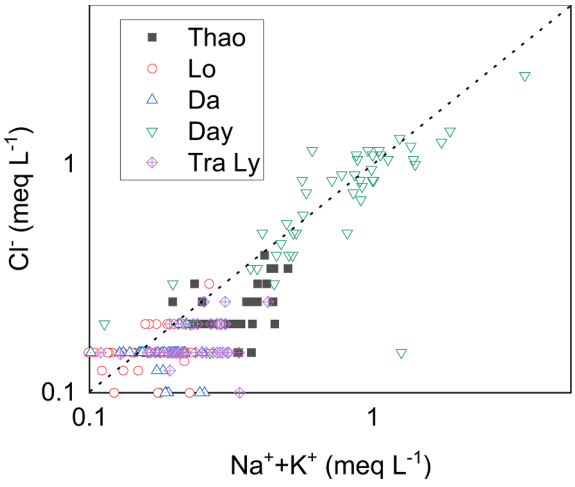

Fig. 5. $[Na^+{+}K^+]$ versus Cl^- in Thao, Lo, Da, Day and Tra Ly sub-basins; the charge imbalances occur mostly in the Thao sub-basin.

where the Thao and Da exhibit an equivalent imbalance between [$Na^+ + K^+$] and Cl^-. In the Day tributary, the charge balance suggests that these ions are generally produced from the same sources. However, as discussed above, weathering may not be the sole process responsible for the production of these ions. Anthropogenic activities are likely to be dominant as evidenced by the observation of concentrated (diluted) Na^+, K^+, and Cl^- during the dry (rainy) season (Fig. 3e, f, i, Table 2), indicating dilution rather than weathering of evaporite rock, which requires water.

Fig. 4 demonstrates that the ions associated with alkaline salt dissolution (Cl^-, Na^+, and K^+) are relatively more concentrated than the ones reported in Moon et al. (2007) and we suspect that lower pH, increasing submersed soil (Nguyen et al., 2021), and increasing bare land (Liu et al., 2021) in the Red River basin have collectively contributed to increased salt/evaporite dissolution. To conclude, evaporite weathering has been intensified by multiple factors, mostly linked to anthropogenic activities (e.g., reservoir building, deforestation, mining), resulting in decadal-scale increases of Na^+, K^+, and Cl^- in the Red River system. Records of rainwater acidity (EANET, 2021) further support this trend, showing a steady increase over the past two decades. Specifically, nitric and sulfuric acids were respectively about 10 and 25 μmol/L in the early 2000 s and 40 and 40 μmol/L in the recent years.

Sulfate in river waters can originate from various sources, including the dissolution of gypsum, oxidation of pyrite, pollution, volcanism, rainout of natural biogenic emissions, and cyclic salt, with the dissolution of gypsum and oxidation of pyrite being the most significant rock weathering sources (Bricker, 1988). An assessment of the significance of pyrite (FeS_2) oxidation and gypsum ($CaSO_4$) dissolution relative to weathering reactions involving carbonic acid can be made by examining the charge balance between [$Ca^{2+} + Mg^{2+}$] and HCO_3^-. Weathering of carbonates or Ca–Mg-silicates by carbonic acid generates equivalent charge units of [$Ca^{2+} + Mg^{2+}$] and HCO_3^-. On the other hand, gypsum dissolution and weathering of carbonates or Ca–Mg-silicates by sulfuric acid results in an excess of [$Ca^{2+} + Mg^{2+}$] over HCO_3^-.

Results of the equivalent comparison tests between alkaline earth cation(s) and HCO_3^-, as well as SO_4^{2-} anion(s) to assess the significance of SO_4^{2-} in different tributaries are shown in Fig. 6 and Table 3. [Ca^{2+}+ Mg^{2+}] and [HCO_3^-+SO_4^{2-}] are statistically equivalent for the five tributaries (Table 3). This suggests that gypsum dissolution and/or pyrite oxidation, along with carbonic acid mediated reactions dominate. Similarly, in the Tra Ly tributary, an equilibrium between [Ca^{2+}+Mg^{2+}] and [HCO_3^-+SO_4^{2-}] indicates its connection with the upstream tributaries. However, in the Day tributary, no weathering process is statistically significant, although the carbonate and gypsum weathering appear to be dominant (indicated by the S-value of [Ca^{2+}+Mg^{2+}] vs [HCO_3^-+SO_4^{2-}], which is the highest among the cation–anion comparison pairs).

Table 3
Paired sample tests for carbonate and gypsum dissolution.

	Thao	Lo	Da	Day	Tra Ly
Ca^{2+} vs HCO_3^-	2.0E-21	5.9E-24	1.8E-15	8.0E-5	2.4E-24
[Ca^{2+}+Mg^{2+}] vs HCO_3^-	1.0E-17	8.8E-7	0.001	2.0E-13	8.9E-7
[Ca^{2+}+Mg^{2+}] vs [HCO_3^-+SO_4^{2-}]	0.76*	0.28*	0.77*	0.031	0.71

* NOT significantly different at 0.05 level; Prob>|t|.

As illustrated in Fig. 6 we assess that the Thao River is dominated by sulfuric acid + carbonic acid mediated reactions, while the Lo and Da Rivers are mainly dominated by carbonic acid mediated reactions. Additionally, the enrichment of SO_4^{2-} in the Day must be associated with anthropogenic impacts. In fact, as shown in Fig. 2j, SO_4^{2-} in the Da and Lo tributaries (about 50 μmol/L) is lower than the global average (Gaillardet et al., 1999) and falls within a similar range as regional rainwater (40 μmol/L (EANET, 2021)). Therefore, atmospheric input is likely to be the main source of SO_4^{2-} in these two upstream tributaries. In addition, the closeness to the equimolar line of the [Ca^{2+}+Mg^{2+}] vs [HCO_3^-+SO_4^{2-}] data points (Fig. 6) implies that no sub-basin exhibits a clear dominance of ion exchange or reverse ion exchange (Subramani et al., 2009). In fact, the plot of [($Ca^{2+} + Mg^{2+}$) − ($HCO_3^- + SO_4^{2-}$)] versus [($Na^+ + K^+$) − Cl^-] (supporting information Figure S4) shows data points centred

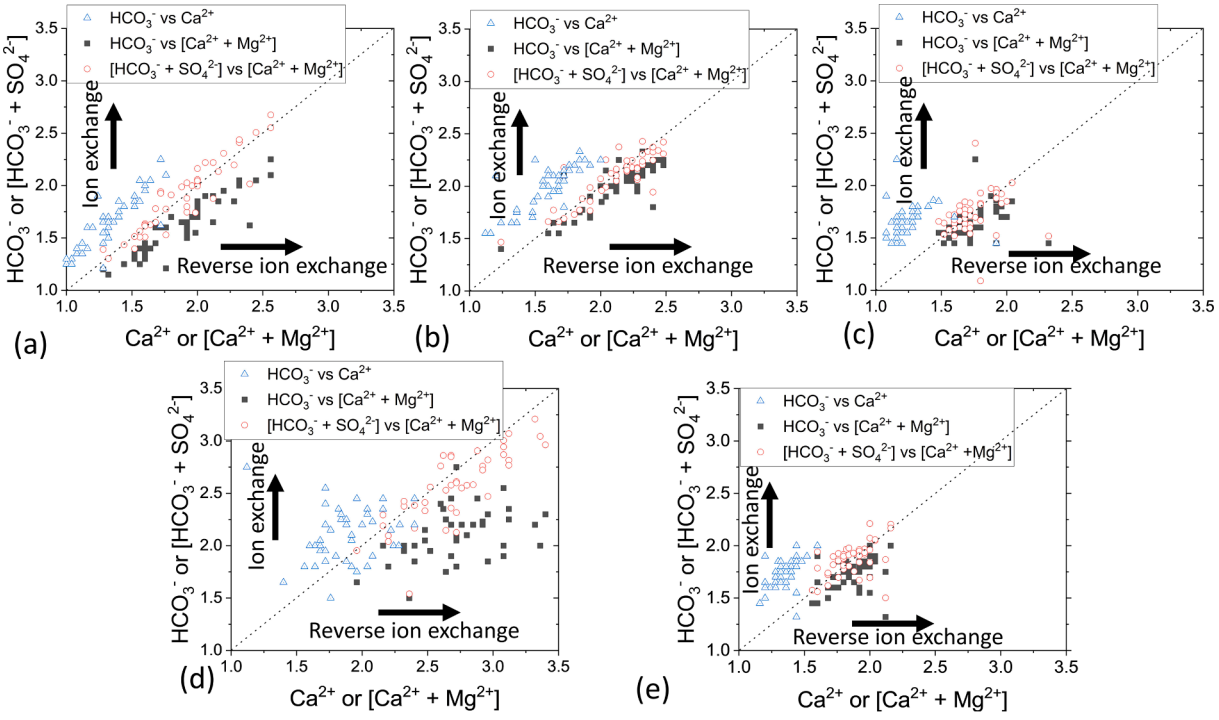

Fig. 6. Alkaline earths (Ca^{2+} or [Ca^{2+}+Mg^{2+}]) versus bicarbonate and sulfate in molarity in different tributaries; (a) Thao, (b) Lo, (c) Da, (d) Day, and (e) Tra Ly sub-basins.

around zero, indicating that the river water chemistry in the RRB is not controlled by (reverse) ion exchanges (Refat Nasher & Humayan Ahmed, 2021). Moreover, the scatter of data points, especially for the Day sub-basin, suggests that other processes or sources rather than ion exchanges dominate the river water chemistry. For the Day River, the data suggests that besides weathering, other processes/solutes contribute to a large deviation from the equimolar line. Notably, NO_3^- in the Day tributary fall within the same range as SO_4^{2-} and SiO_2 (Luu et al., 2021). Nitrate and many other solutes deriving from anthropogenic activities are independent of weathering, leading to data scattering around the equimolar line (Fig. 6d). More broadly, anthropogenic impacts outweigh weathering contributions in the RRD region (Day). In the Thao tributary, we suspect that mining activities in coal-bearing and sulfide-bearing deposits along the RRFZ induce pyrite oxidation (Liu et al., 2021; Yang et al., 2014), likely accounting for the higher SO_4^{2-} in the Thao than in Lo and Da (Fig. 2j).

Distinguishing between gypsum and pyrite sources of SO_4^{2-} is challenging because pyrite oxidation generates sulfuric acid, which in turn can weather surrounding carbonate and silicate minerals.

The carbonate – evaporite – silicate end member ternary analysis (Fig. 7) demonstrates that no tributary in the Red River system shows evidence of gypsum dissolution indicated by the absence of data clusters near the ($Cl + SO_4^{2-}$) apex. The data from the Day River predominantly align along the Alk – [$Cl^- + SO_4^{2-}$] axis, indicating dominance of anthropogenic inputs with limited silicate production. In contrast, the Thao River is characterized by pyrite oxidation with concomitant silicate weathering as indicated by data plotting toward the center of the ternary diagram. The Lo River has the least SO_4^{2-} and SiO_2 weathering, with data clustering near the Alk axis. Furthermore, the ternary diagram (Fig. 7) also shows that Si weathering is most prevalent in the Thao tributary whereas there is a net loss of Si in the delta region due to high biological activities and negligible silicate weathering.

The calcite saturation index (CSI) exhibits variation, ranging from oversaturation in the Lo and Tra Ly tributaries (two thirds of the samples are oversaturated) to saturation in the Da and Day tributaries (half of the samples are oversaturated) and undersaturation in the Thao (two fifths of the samples are oversaturated) (Fig. 8). Overall, 58 % of samples were oversaturated with calcite. This trend is generally in agreement with

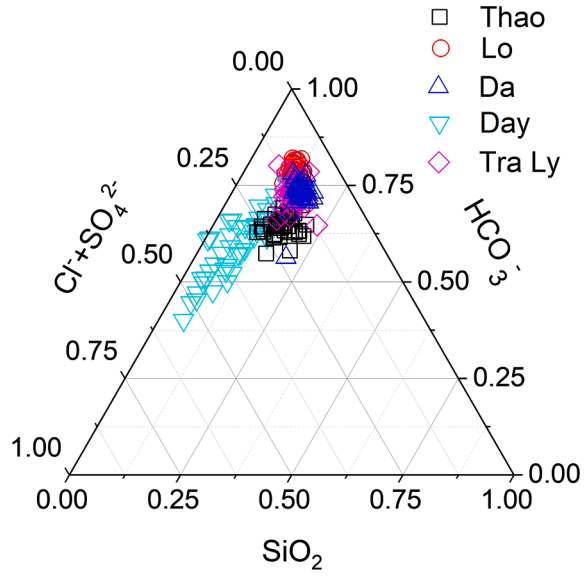

Fig. 7. Carbonate – evaporite – silicate end member ternary plot (Chai et al., 2024); pyrite oxidation and silicate weathering likely occur in the Thao tributary; calcite and dolomite dissolution likely occurs in the Lo tributary, pyrite oxidation and carbonate weathering likely occurs in the Day tributary. The Da and Tra Ly tributaries are intermediate between the Thao and Lo tributaries.

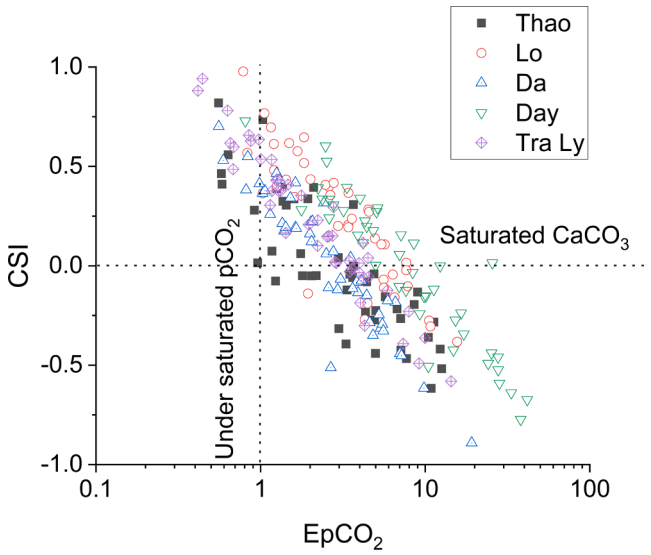

Fig. 8. CSI versus $EpCO_2$ in different sub-basins of the Red River system, water is mostly over saturated with CO_2 and in equilibrium with calcite.

earlier observations of Moon et al. (2007) who found CSI oversaturation in half of their samples. A paired *t*-test showed that CSI was higher in summer than winter samples, which we attribute to variability in pH. Based on the CSI data, we infer that $CaCO_3$ tends to dissolve in mining and deforested tributaries such as the Thao while secondary precipitation tends to occur in carbonate rich tributaries like the Lo tributary. The oversaturated CSI in the Lo tributary, characterized by a thick marine succession of Triassic limestone and fine-grained clastic rocks, suggests that carbonate weathering is not favored in this sub-basin.

The excess carbon dioxide partial pressure ($EpCO_2$) predominantly exceeds unity and is particularly high in the populous-urbanized catchment of the Day River (Fig. 8; Salgado et al., 2022). Comparing our findings for the upstream tributaries with those of Moon et al. (2007), we note an increase in $EpCO_2$, which stimulates CO_2 evasion to the atmosphere and shifts the [$Ca^{2+} + Mg^{2+}$] – HCO_3^- equivalent balance further towards [$Ca^{2+} + Mg^{2+}$] than HCO_3^- (Fig. 6). This tilting may be explained by a coupling between pyrite oxidation and silicate dissolution. Pyrite oxidation, along with concurrent silicate weathering, generates sulfate (increased SO_4^{2-}), neutralizes the alkalinity (decreased HCO_3^-), and dissolves silicates (elevated SiO_2). The equivalent plot (Fig. 6d) also shows an imbalance/ non-alignment between cations and anions in the Day catchment. We propose that in this delta region, the balance between photosynthetic productivity, respiration/biodegradation and the dynamic state of river flow (i.e. autochthonous processes), instead of carbonate weathering (an allochthonous process), determine its pCO_2 level (Salgado et al., 2022; Stallard & Edmond, 1983).

4.3. Denudation in the Red River system

Overall, the interpretations above suggest that weathering processes play a trivial role in the delta region. Therefore, in this subsection, we shift our focus to denudation processes taking place in the three upstream sub-basins; Thao, Lo, and Da. Moon et al. (2007) found that the TDS yield in the upstream mountain area of the Red River was 0.2–2.2 x 10^6 mol km^{-2} yr^{-1} in winter and 2.3–8.3 x 10^6 mol km^{-2} yr^{-1} in summer. Our data show an average TDS yield of 1.2 ± 1.2, 2.9 ± 1.8, and 2.7 ± 2.4 x 10^6 mol km^{-2} yr^{-1} in the Thao, Lo, and Da tributaries, respectively, reaching as high as 11.4 x 10^6 mol km^{-2} yr^{-1} in the summer and 2.4 x 10^6 mol km^{-2} yr^{-1} in the winter (Fig. 9a). A nonparametric paired sample signed test shows that TDS in the Thao is significantly lower due to the dominance of silicate/quartz igneous rocks than the other two upstream sub-basins dominated by evaporite rock (Burchfiel & Wang,

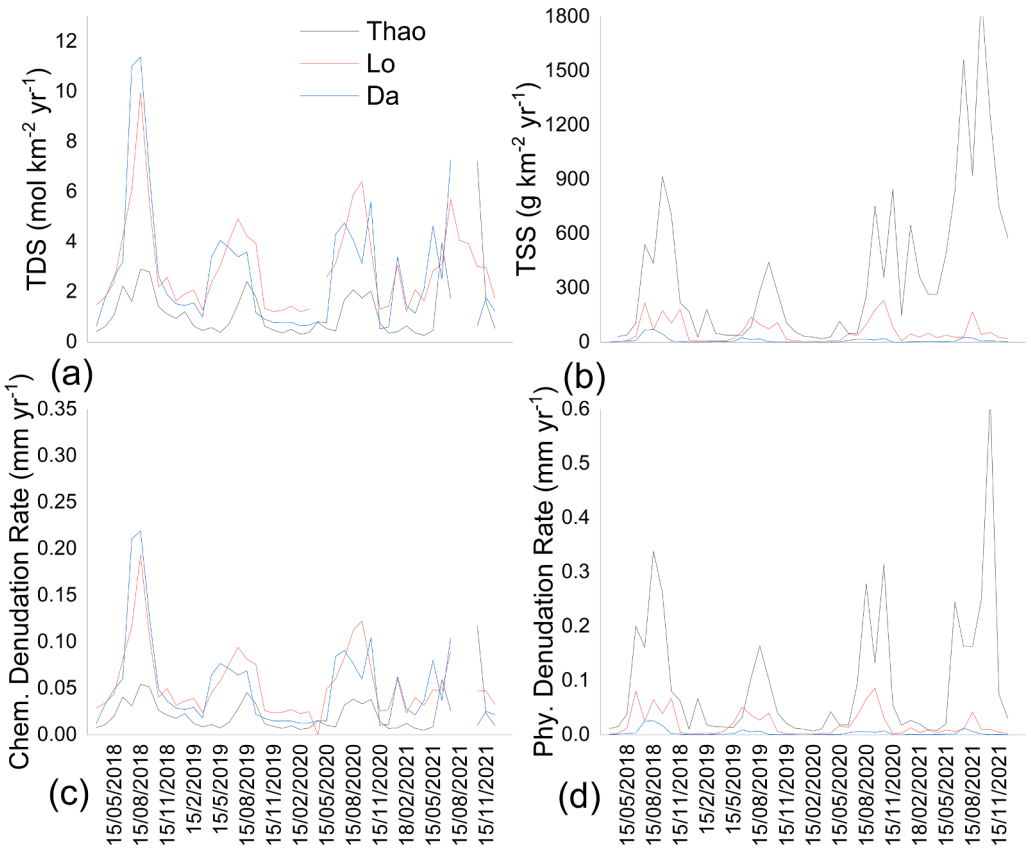

Fig. 9. (a) TDS yield, (b), TSS yield at the outflow of sub-basins, (c) Chemical denudation rate calculated from TDS data and (d) physical denudation rate calculated from TSS data.

2003; Leloup et al., 1995; Wang et al., 2005). Despite similar catchment areas, discharge in the Da sub-basin is nearly three times higher than in the Thao sub-basin, resulting in a notably higher TDS yield in the Da than in the Thao (Trinh & Do, 2022). Furthermore, the construction of reservoirs over the past two decades in the Da and Lo sub-basins has increased the land submersed under water, facilitating the dissolution of evaporite materials (Nguyen et al., 2021).

Compared to other global rivers, the TDS yield was similar to those sourced in the Himalayas-Tibetan Plateau (Upper Huang He: 0.56–1.5, Ganges–Brahmaputra: 1.7–5.7, and Indus: 1.3 x 10^6mol km^{-2} yr^{-1}) (Dalai et al., 2003; Galy et al., 1999; Karim & Veizer, 2000; Wu et al., 2005) as well as other rivers draining orogenic zones such as the Amazon (0.59–4.1) x 10^6 mol km^{-2} yr^{-1} and Mackenzie (0.5–4.9) x 10^6 mol km^{-2} yr^{-1}, but higher than the Orinoco (0.96–1.6) x 10^6 mol km^{-2} yr^{-1} draining the Andes, or rivers of the Russian Far East draining the collision zone (0.04–0.38) x 10^6 mol km^{-2} yr^{-1} (Edmond et al., 1996; Galy et al., 1999; Stallard & Edmond, 1983). In contrast, rivers draining shield terrains have a low TDS yield – e.g., the Amazon draining the Brazilian Shield 0.3 x 10^6 mol km^{-2} yr^{-1}, Orinoco draining the Guayana Shield (0.01–0.6) x 10^6 mol km^{-2} yr^{-1}, St. Lawrence draining the Canadian Shield (0.04–0.07) x 10^6 mol km^{-2} yr^{-1}, or the rivers draining the Siberian Shield (0.09–1.5 x 10^6 mol km^{-2} yr^{-1}) (Edmond et al., 1995; Gaillardet et al., 1997; Huh & Edmond, 1999; Millot et al., 2003).

Assuming that the density of rock is 2.7 g cm^{-3} (Moon et al., 2007), we calculated the chemical denudation rate in the Red River basin from the TDS yield (Fig. 9c). The average chemical denudation rates of the Thao, Lo, and Da sub-basins are 0.022 ± 0.021, 0.055 ± 0.035, and 0.051 ± 0.047 mm yr^{-1}, respectively, and comparable to values reported in (Moon, et al., 2007); 0.080 mm yr^{-1} in summer and 0.020 mm yr^{-1} in winter.

The total suspended solid (TSS) yield is high in the Thao and low in the Lo and Da tributaries (Fig. 9b). Our analysis suggests that reservoirs

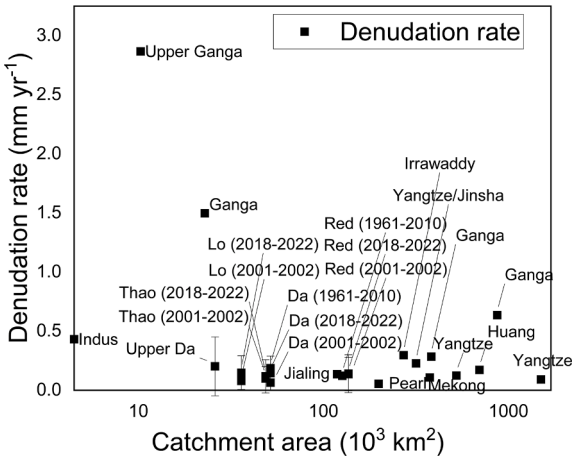

Fig. 10. Denudation rates calculated from total material loads for Asian rivers stemming from Tibetan Plateau versus their catchment area as courtesy from (Moon et al., 2007; Vinh et al., 2014; Wittmann et al., 2020), and this study.

in the Red River system have been highly effective in retaining TSS (Dang et al., 2010; Nguyen et al., 2021), as indicated by the low TSS levels observed in Da and Lo. We also estimated the physical denudation rate for each sub-basins using their respective TSS data (Fig. 9d).

Fig. 10 shows two ranges of denudation rates in Asian river catchments. The first is rivers draining the Indian sub-continent, Indus, Ganga and Irrawaddy, characterized mainly by an annual denudation rate > 0.2 mm yr^{-1} and the second is rivers flowing to the Pacific Ocean, characterized mostly by a denudation rate < 0.2 mm yr^{-1} (Chai et al., 2024). The Red River logically belongs to the second range, having

annual mean total denudation rates between 0.064 and 0.187 mm yr^{-1}. Regionally, together with our calculated data, we observe a high denudation rate in upstream/head water catchments (e.g. Upper Ganga, Indus, and Upper Da) and low denudation rate in large scale basins –, i.e. a negative correlation between denudation rate and catchment area. Specific to the sub-basins and catchments in the Red River basin, total denudation rate was higher in the 1961–2010 period than in 2018–2022; implying that the impoundment practice which has intensified since the 2000 s has lowered the particulate material transport (McGowan et al., 2023). In addition, our calculated denudation rates for the Da and Lo (two heavily impounded rivers) in 2018–2022 are higher than the values of 2001–2002 reported in Moon et al. (2007). Our calculation has already tried to account for the impoundment effect by integrating the chemical denudation rates from these sub-basins with the physical denudation rate calculated for the least impounded (Thao) sub-basin. However, the overall annual total denudation rate for the whole Red River basin denoted as "Red" in Fig. 10 is statistically similar between the different data sets: 0.122, 0.141 ± 0.161, and 0.136 ± 0.142 mm yr^{-1} for 1961–2010, 2001–2002, and 2018–2022, respectively.

Investigating further, the calculated rates from our study for similar sites downstream of major reservoirs are comparable to those reported by Moon et al. (2007). During 2001–2002, for the Da River, the summer and winter rates were 0.041 and $4.0E^{-4}$ mm yr^{-1} respectively; for the Lo River, the corresponding rates were 0.029 and 0.005 mm yr^{-1}; for the Thao River, the rates were 0.109 and 0.013 mm yr^{-1}, respectively. Our data show that the summer and winter rates are, respectively, about $6.5E^{-3}$ and $9.0E^{-4}$ mm yr^{-1} for the Da River, 0.029 and $6.4E^{-3}$ mm yr^{-1} for the Lo River, and 0.136 and 0.023 mm yr^{-1} for the Thao River. Moon et al. (2007) suggested that their values are probably underestimates, since the calculation was based on the furthest downstream samples of the Da and the Lo located below reservoirs. For the same reason, the explanation for lower denudation rates in our study of the Da River compared with that of Moon et al. (2007) is that over the last 20 years, more dams have been built along the Da River (Nguyen et al., 2021), which retain TSS. Otherwise, the physical denudation rate in the Thao is relatively higher than the ones reported by Moon et al. (2007) (the rate calculated for the other two tributaries is unreliable due to TSS retention in reservoirs). We suspect that the physical denudation rate in the Red River system has increased recently. The reasons could be deforestation, urbanization, and climate change induced extreme events (McElwee et al., 2016).

We opted to utilize the physical denudation rate of the Thao tributary for all sub-basins since the rates calculated from TSS of the Da and Lo tributaries are heavily influenced by reservoir retention. The average total denudation rate in the three tributaries (Thao, Lo, and Da) is calculated as 0.107 ± 0.108, 0.137 ± 0.129, and 0.139 ± 0.137 mm yr^{-1}, respectively which is comparable to the findings of Moon et al. (2007).

Moon et al. (2007) noted that their calculated total denudation rate is comparable to the estimate from Pleistocene sediment volumes in the Red River basin (0.178 mm yr^{-1}) (Clift et al., 2006) and much lower than maximum total denudation rates in the southern and western syntaxes of the Himalayas – 10 mm yr^{-1} for the Namche Barwa determined by fission track (Burg et al., 1998) and 3–5 mm yr^{-1} for the Nanga Parbat calculated from mineral cooling ages (Moore & England, 2001). Moon et al. (2007) concluded that this is probably due to the exceptionally focused erosion in the syntaxes of the Himalayas. While we agree with that conclusion, we suspect that the actual denudation rate might have been higher, considering that the monitoring sites are located at the outlets of high Strahler order catchments where sand mining and reservoir dams have greatly reduced TSS yield (Dang et al., 2010).

5. Conclusions

Over a meticulous four-year survey spanning from 2018 to 2022, we observed significant shifts in the water chemistry of the Red River. Depleted SiO_2 levels, attributed to heightened rates of aquatic biological uptake surpassing silicate weathering, were notable, alongside enriched CO_2 due to organic matter mineralization. Moreover, concentrations of evaporite ions (Na^+, K^+, and Cl^-) have increased markedly. The transformation in water chemistry over the last 20 years has seen the river's pH transition from slightly alkaline to circumneutral, driven by a multitude of anthropogenic activities. In contrast to other large Asian rivers in arid regions (Chai et al., 2024), the construction of hydropower dam and mining activities have led to discernible differences among mountain tributaries, with pristine areas giving way to evaporite dominance in urbanized regions. Chemical denudation rates have surged in soil-submerged regions, while physical denudation rates have risen along the RRFZ. The imbalance between major cations and anions at urbanized sites underscores the direct inputs of anthropogenic waste. Notably, the observed decline in pH mirrors trends observed in other major river systems across the region which all stem from the Tibetan Plateau and flow through densely populated areas (Guo et al., 2015), indicating a broader pattern of anthropogenic-driven shifts from carbonate to evaporite dominance.

CRediT authorship contribution statement

Duc A. Trinh: Writing – original draft, Visualization, Validation, Methodology, Funding acquisition, Formal analysis, Data curation, Conceptualization. **Nga T. Do:** . **Virginia N. Panizzo:** Writing – review & editing, Methodology, Investigation, Formal analysis. **Suzanne McGowan:** Writing – review & editing, Validation, Methodology, Investigation, Conceptualization. **Jorge Salgado:** Writing – review & editing, Visualization, Methodology. **Andy R.G. Large:** Supervision, Resources, Project administration, Methodology, Funding acquisition, Conceptualization. **Andrew C.G. Henderson:** Project administration, Investigation, Funding acquisition, Formal analysis, Data curation. **Thuy T. Vu:** Visualization, Data curation.

Declaration of competing interest

The authors declare that they have no known competing financial interests or personal relationships that could have appeared to influence the work reported in this paper.

Data availability

All water chemistry data are openly accessible in: https://doi.org/10.25405/data.ncl.25075583

Acknowledgments

The fieldwork and laboratory analyses were consecutively conducted within the frameworks of the NERC-NAFOSTED NE/P014577/1, the UKRI GCRF Living Deltas Hub NE/S008926/1 and the MOST-OeAD NĐT/AT/22/27 research projects.

Open Research.

Data - All water chemistry data are openly accessible in: Doi: 10.25405/data.ncl.25075583

Appendix A. Supplementary material

Supplementary data to this article can be found online at https://doi.org/10.1016/j.jaesx.2024.100183.

References

Berner, R.A., 1971. Worldwide sulfur pollution of rivers. J. Geophys. Res. 76 (27), 6597–6600. https://doi.org/10.1029/jc076i027p06597.

Bricker, O.P., 1988. The Global Water Cycle Geochemistry and Environment. Eos Transactions. Am. Geophys. Union 64 (4).

Burchfiel, B.C., Wang, E., 2003. Northwest-trending, middle Cenozoic, left-lateral faults in southern Yunnan, China, and their tectonic significance. J. Struct. Geol. 25 (5), 781–792. https://doi.org/10.1016/s0191-8141(02)00065-2.

Burg, J.-P., Nievergelt, P., Oberli, F., Seward, D., Davy, P., Maurin, J.-C., Diao, Z., Meier, M., 1998. The Namche Barwa syntaxis: evidence for exhumation related to compressional crustal folding. J. Asian Earth Sci. 16 (2–3), 239–252. https://doi.org/10.1016/s0743-9547(98)00002-6.

Chai, N., Zhao, Z., Li, X., Xiao, J., & Jin, Z. (2024). Chemical weathering processes in the Chinese Loess Plateau. Geoscience Frontiers, 15(5), 101842. https://doi.org/Doi: 10.1016/j.gsf.2024.101842.

Chen, J., He, D., Cui, S., 2003. The response of river water quality and quantity to the development of irrigated agriculture in the last 4 decades in the Yellow River Basin, China. Water Resour. Res. 39 (3), 10.1029/2001WR001234.

Claudi, R., Graves, A., Taraborelli, A.C., Prescott, R., Mastitsky, S., 2012. Impact of pH on survival and settlement of dreissenid mussels. Aquat. Invasions 7 (1), 21–28. https://doi.org/10.3391/ai.2012.7.1.003.

Clesceri, L. S., Greenberg, A. E., & Eaton, A. D. (1998). Standard Methods for the Examination of Water and Waste Water. (20th Editi). APHA American Public Health Association.

Clift, P.D., Carter, A., Campbell, I.H., Pringle, M.S., Van Lap, N., Allen, C.M., Hodges, K. V., Tan, M.T., 2006. Thermochronology of mineral grains in the Red and Mekong Rivers, Vietnam: Provenance and exhumation implications for Southeast Asia. Geochem. Geophys. Geosyst. 7 (10) https://doi.org/10.1029/2006gc001336.

Dalai, T.K., Krishnaswami, S., Kumar, A., 2003. Sr and 87Sr/86Sr in the Yamuna River System in the Himalaya: sources, fluxes, and controls on sr isotope composition. Geochim. Cosmochim. Acta 67 (16), 2931–2948. https://doi.org/10.1016/s0016-7037(03)00203-5.

Dang, T.H., Coynel, A., Orange, D., Blanc, G., Etcheber, H., Le, L.A., 2010. Long-term monitoring (1960–2008) of the river-sediment transport in the Red River Watershed (Vietnam): Temporal variability and dam-reservoir impact. Sci. Total Environ. 408 (20), 4654–4664. https://doi.org/10.1016/j.scitotenv.2010.07.007.

Dos Reis Oliveira, P.C., van der Geest, H.G., Kraak, M.H.S., Verdonschot, P.F.M., 2019. Land use affects lowland stream ecosystems through dissolved oxygen regimes. Sci. Rep. 9 (1), 19685. https://doi.org/10.1038/s41598-019-56046-1.

Drake, T.W., Raymond, P.A., Spencer, R.G.M., 2017. Terrestrial carbon inputs to inland waters: A current synthesis of estimates and uncertainty. Limnol. Oceanogr. Lett. 3 (3), 132–142. https://doi.org/10.1002/lol2.10055.

Drogue, C., Cat, N.N., Dazy, J., 2000. Geological factors affecting the chemical characteristics of the thermal waters of the carbonate karstified aquifers of Northern Vietnam. Hydrol. Earth Syst. Sci. 4 (2), 332–340. https://doi.org/10.5194/hess-4-332-2000.

Duc, T.A., Vachaud, G., Bonnet, M.P., Prieur, N., Loi, V.D., Anh, L.L., 2007. Experimental investigation and modelling approach of the impact of urban wastewater on a tropical river; a case study of the Nhue River, Hanoi, Viet Nam. J. Hydrol. 334 (3–4), 347–358. https://doi.org/10.1016/j.jhydrol.2006.10.022.

Duc, T.A., Giang, N.H., Vachaud, G., Choi, S.U., 2009. Application of excess carbon dioxide partial pressure (EpCO2) to the assessment of trophic state of surface water in the Red River delta of Vietnam. Int. J. Environ. Stud. 66 (1), 27–47. https://doi.org/10.1080/00207230902760473.

Duc, T.A., Nga, D.T., Panizzo, V.N., McGowan, S., Leng, M.J., Trinh, A.D., Do, T.N., Panizzo, V.N., McGowan, S., Leng, M.J., 2020. Using stable isotopes to estimate young water fractions in a heavily regulated, tropical lowland river basin. Hydrol. Process. 34 (22), 4239–4250. https://doi.org/10.1002/hyp.13878.

Duong, T.T., Nguyen, H.Y., Nguyen, T.K., Dang, D.K., Tran, T.T.H., Le, T.P.Q., Le, N.D., Panizzo, V., McGowan, S., Nguyen, T.K., Tran, T.T.H., Le, N.D., Dang, D.K., Vu, T.N., Panizzo, V., McGowan, S., 2019. Transitions in diatom assemblages and pigments through dry and wet season conditions in the Red River, Hanoi (Vietnam). Plant Ecology and Evolution 152 (2), 163–177. https://doi.org/10.5091/plecevo.2019.1627.

EANET. (2021). Acid Deposition Monitoring Network in East Asia. https://monitoring.eanet.asia/document/public/index.

Edmond, J.M., Palmer, M.R., Measures, C.I., Grant, B., Stallard, R.F., 1995. The fluvial geochemistry and denudation rate of the Guayana Shield in Venezuela, Colombia, and Brazil. Geochim. Cosmochim. Acta 59 (16), 3301–3325. https://doi.org/10.1016/0016-7037(95)00128-m.

Edmond, J.M., Palmer, M.R., Measures, C.I., Brown, E.T., Huh, Y., 1996. Fluvial geochemistry of the eastern slope of the northeastern Andes and its foredeep in the drainage of the Orinoco in Colombia and Venezuela. Geochim. Cosmochim. Acta 60 (16), 2949–2974. https://doi.org/10.1016/0016-7037(96)00142-1.

Gaillardet, J., Dupre, B., Allegre, C.J., Négrel, P., 1997. Chemical and physical denudation in the Amazon River Basin. Chem. Geol. 142 (3–4), 141–173. https://doi.org/10.1016/s0009-2541(97)00074-0.

Gaillardet, J., Dupré, B., Louvat, P., Allègre, C.J., 1999. Global silicate weathering and CO2 consumption rates deduced from the chemistry of large rivers. Chem. Geol. 159 (1–4), 3–30. https://doi.org/10.1016/s0009-2541(99)00031-5.

Galloway, J.N., 2001. No Title. Water Air Soil Pollut. 130 (1/4), 17–24. https://doi.org/10.1023/a:1012272431583.

Galy, A., France-Lanord, C., Derry, L.A., 1999. The strontium isotopic budget of Himalayan rivers in Nepal and Bangladesh. Geochim. Cosmochim. Acta 63 (13–14), 1905–1925. https://doi.org/10.1016/s0016-7037(99)00081-2.

Global Forest Watch. (2024). https://www.globalforestwatch.org/dashboards/country/CHN/30/?category=land-use.

Guo, J., Wang, F., Vogt, R.D., Zhang, Y., Liu, C.-Q., 2015. Anthropogenically enhanced chemical weathering and carbon evasion in the Yangtze Basin. Sci. Rep. 5, 11941. https://doi.org/10.1038/srep11941.

Hoang, Thi Thu Ha; Le, Thi Phuong Quynh; Le, N. Da. (2020). Preliminary assessment of factors impacting on bicarbonate Concentrations in the Red River System. Journal of Analytical Science, 25(4), 1–6.

Huh, Y., Edmond, J.M., 1999. The fluvial geochemistry of the rivers of Eastern Siberia: III. Tributaries of the Lena and Anabar draining the basement terrain of the Siberian Craton and the Trans-Baikal Highlands. Geochim. Cosmochim. Acta 63 (7–8), 967–987. https://doi.org/10.1016/s0016-7037(99)00045-9.

Joern, K., Steffen, G., & Le, T. L. (2024). Province Nam Dinh -Analysis for a future integrated water resource. http://www.idm.gov.vn/nguon_luc/Xuat_ban/2006/B27/b87.htm.

Karim, A., Veizer, J., 2000. Weathering processes in the Indus River Basin: implications from riverine carbon, sulfur, oxygen, and strontium isotopes. Chem. Geol. 170 (1–4), 153–177. https://doi.org/10.1016/s0009-2541(99)00246-6.

Kubo, A., Kawarasaki, K., Hara, H., 2022. Silica removal at sewage treatment plants causes new silica deficiency. Sci. Rep. 12 (1), 8141. https://doi.org/10.1038/s41598-022-12272-8.

Le, T.P.Q., Marchand, C., Ho, C.T., Le, N.D., Duong, T.T., Lu, X., Doan, P.K., Nguyen, T. K., Nguyen, T.M.H., Vu, D.A., 2018. CO2 partial pressure and CO2 emission along the lower Red River (Vietnam). Biogeosciences 15 (15), 4799–4814. https://doi.org/10.5194/bg-15-4799-2018.

Leloup, P.H., Lacassin, R., Tapponnier, P., Schärer, U., Zhong, D., Liu, X., Zhang, L., Ji, S., Trinh, P.T., 1995. The Ailao Shan-Red River shear zone (Yunnan, China), Tertiary transform boundary of Indochina. Tectonophysics 251 (1–4), 3–84. https://doi.org/10.1016/0040-1951(95)00070-4.

Li, T., 2016. A Historical Sketch of the Landscape of the Red River Delta. TRaNS: Trans -Regional and -National Studies of Southeast. Asia 4 (2), 351–363. https://doi.org/10.1017/trn.2016.8.

Li, M., Peng, C., Wang, M., Xue, W., Zhang, K., Wang, K., Shi, G., Zhu, Q., 2017. The carbon flux of global rivers: A re-evaluation of amount and spatial patterns. Ecol. Ind. 80, 40–51. https://doi.org/10.1016/j.ecolind.2017.04.049.

Liu, F., Wang, W., Wang, J., Zhang, X., Ren, J., Liu, Y., 2021. Multi-scale analysis of the characteristics of the changing landscape of the typical mountainous region of Southwest China over the past 40 years. PeerJ 9, e10923–e. https://doi.org/10.7717/peerj.10923.

Luu, M.T.N., Dinh, T.D., Trinh, D.A., Do, N.T., 2021. Water quality in an urbanized river basin impacted by multi-pollution sources: From comprehensive surveys to modelling. ScienceAsia 47 (1), 86–95. https://doi.org/10.2306/scienceasia1513-1874.2021.014.

Luu, T.N.M., Garnier, J., Billen, G., Orange, D., Némery, J., Le, T.P.Q., Tran, H.T., Le, L. A., 2010. Hydrological regime and water budget of the Red River Delta (Northern Vietnam). J. Asian Earth Sci. 37 (3), 219–228. https://doi.org/10.1016/j.jseaes.2009.08.004.

Maavara, T., Dürr, H. H., & Van Cappellen, P. (2014). Worldwide retention of nutrient silicon by river damming: From sparse data set to global estimate. Global Biogeochemical Cycles, 28(8), 842–855. https://doi.org/Doi: 10.1002/2014GB004875.

McElwee, P., Nghiem, T., Le, H., Vu, H., 2016. Flood vulnerability among rural households in the Red River Delta of Vietnam: implications for future climate change risk and adaptation. Nat. Hazards 86 (1), 465–492. https://doi.org/10.1007/s11069-016-2701-6.

McGowan, S., Large, A., Henderson, A.C.G.G., Wallerstein, N., 2023. Dammed deltas: Sinking Asian deltas in a warming world. One Earth 6 (3), 195–199. https://doi.org/10.1016/j.oneear.2023.02.013.

Meybeck, M., 2002. Riverine quality at the Anthropocene: Propositions for global space and time analysis, illustrated by the Seine River. Aquat. Sci. 64 (4), 376–393. https://doi.org/10.1007/pl00012593.

Michel, M., 1987. Global chemical weathering of surficial rocks estimated from river dissolved loads. Am. J. Sci. 287 (5), 401–428. https://doi.org/10.2475/ajs.287.5.401.

Millot, R., Gaillardet, J. érôm., Dupré, B., & Allègre, C. J. (2003). Northern latitude chemical weathering rates: clues from the Mackenzie River Basin, Canada. Geochimica et Cosmochimica Acta, 67(7), 1305–1329. Doi: 10.1016/s0016-7037(02)01207-3.

Moon, S., Huh, Y., Qin, J., van Pho, N., 2007. Chemical weathering in the Hong (Red) River basin: Rates of silicate weathering and their controlling factors. Geochim. Cosmochim. Acta 71 (6), 1411–1430. https://doi.org/10.1016/j.gca.2006.12.004.

Moore, M.A., England, P.C., 2001. On the inference of denudation rates from cooling ages of minerals. Earth Planet. Sci. Lett. 185 (3–4), 265–284. https://doi.org/10.1016/s0012-821x(00)00380-0.

Moore, J., Fanelli, R.M., Sekellick, A.J., 2019. High-Frequency Data Reveal Deicing Salts Drive Elevated Specific Conductance and Chloride along with Pervasive and Frequent Exceedances of the U.S. Environmental Protection Agency Aquatic Life Criteria for Chloride in Urban Streams. Environ. Sci. Tech. 54 (2), 778–789. https://doi.org/10.1021/acs.est.9b04316.

NCMH. (2017). The Hydrological Regime Along the Marine Coast, North Vietnam in the 2017 Year.

Nguyen, N.L., Do, T.N., Trinh, A.D., 2021. Application of water stable isotopes for hydrological characterization of the red river (Asia). Water (switzerland) 13 (15), 1–15. https://doi.org/10.3390/w13152051.

Nisha, B.K., Balakrishna, K., Udayashankar, H.N., Arun, K., Manjunatha, B.R., 2022. Contribution of dissolved organic carbon from a tropical river system to the Arabian

Sea, southwestern India. Journal of Asian Earth Sciences: X 7, 100085. https://doi.org/10.1016/j.jaesx.2022.100085.
Refat Nasher, N.M., Humayan Ahmed, M., 2021. Groundwater geochemistry and hydrogeochemical processes in the Lower Ganges-Brahmaputra-Meghna River Basin areas, Bangladesh. Journal of Asian Earth Sciences: X 6, 100062. https://doi.org/10.1016/j.jaesx.2021.100062.
Renwick, W. H. (1991). Global freshwater quality: A first assessment. In and R. H. B. B. Michael Meybeck, Deborah Chapman (Ed.), Global Environmental Change (Vol. 1, Issue 4). Oxford. Doi: 10.1016/0959-3780(91)90062-x.
Roberts, L.R., Do, N.T., Panizzo, V.N., Taylor, S., Watts, M., Hamilton, E., McGowan, S., Trinh, D.A., Leng, M.J., Salgado, J., 2022. In flux: Annual transport and deposition of suspended heavy metals and trace elements in the urbanised, tropical Red River Delta. Vietnam. Water Research 224, 119053. https://doi.org/10.1016/j.watres.2022.119053.
Salgado, J., Duc', T. A., Nga, D. T., Panizzo, V. N., Bass, A. M., Zheng, Y., Taylor, S., Roberts, L. R., Lacey, J. H., Leng, M. J., & McGowan, S. (2022). Urbanization and seasonality strengthens the CO_2 capacity of the Red River Delta, Vietnam. Environmental Research Letters, 17(10), 104052. Doi: 10.1088/1748-9326/ac9705.
Scharpenseel, H. W., & Becker-Heidmann, P. (1990). Chapter 1 Overview of the Greenhouse Effect. In Soils on A Warmer Earth - Effects of Expected Climate Change on Soil Processes, with Emphasis on the Tropics and Sub-Tropics, Proceedings of an International Workshop on Effects of Expected Climate Change on Soil Processes in the Tropics and Sub-tropics (pp. 1–14). Elsevier. Doi: 10.1016/s0166-2481(08)70477-x.
Sharma, M.K., Kumar, P., Prajapati, P., Bhanot, K., Wadhwa, U., Tomar, G., Goyal, R., Prasad, B., Sharma, B., 2022. Study of hydrochemical and geochemical characteristics and solute fluxes in Upper Ganga Basin, India. Journal of Asian Earth Sciences: X 8, 100108. https://doi.org/10.1016/j.jaesx.2022.100108.
Stallard, R.F., 1988. Weathering and Erosion in the Humid Tropics. In Physical and Chemical Weathering in Geochemical Cycles. Springer, Netherlands, pp. 225–246.
Stallard, R.F., Edmond, J.M., 1983. Geochemistry of the Amazon: 2. The influence of geology and weathering environment on the dissolved load. J. Geophys. Res. Oceans 88 (C14), 9671–9688. https://doi.org/10.1029/jc088ic14p09671.
Subramani, T., Rajmohan, N., Elango, L., 2009. Groundwater geochemistry and identification of hydrogeochemical processes in a hard rock region. Southern India. Environmental Monitoring and Assessment 162 (1–4), 123–137. https://doi.org/10.1007/s10661-009-0781-4.
Trinh, A.D., Do, T.N., 2022. In: Application of Isotope Techniques for Assessing Hydrology of Red River (asia). International Association for Hydro-Environment Engineering and Research (IAHR). https://doi.org/10.3850/iahr-39wc252171192022647.
Trinh, A.D., Meysman, F., Rochelle-Newall, E., Bonnet, M.P., 2012. Quantification of sediment-water interactions in a polluted tropical river through biogeochemical modeling. Global Biogeochem. Cycles 26 (3), 1–15. https://doi.org/10.1029/2010GB003963.
van Dokkum, H.P., Hulskotte, J.H.J., Kramer, K.J.M., Wilmot, J., 2004. Emission, Fate and Effects of Soluble Silicates (Waterglass) in the Aquatic Environment. Environ. Sci. Tech. 38 (2), 515–521. https://doi.org/10.1021/es0264697.
Varallyay, G., 2010. The impact of climate change on soils and on their water management. Agron. Res. 8, 385–396.
Vinh, V.D., Ouillon, S., Thanh, T.D., Chu, L.V., 2014. Impact of the Hoa Binh dam (Vietnam) on water and sediment budgets in the Red River basin and delta. Hydrol. Earth Syst. Sci. 18 (10), 3987–4005. https://doi.org/10.5194/hess-18-3987-2014.
Vitaly, K., Michel, M., & Ellysar, B. (1998). A Water Quality Assessment of the Former Soviet Union (1st Editio). CRC Press. https://doi.org/Doi: 10.1201/9781482272130.
Wang, C.Y., Zhou, M.-F., Zhao, D., 2005. Mineral chemistry of chromite from the Permian Jinbaoshan Pt–Pd–sulphide-bearing ultramafic intrusion in SW China with petrogenetic implications. Lithos 83 (1–2), 47–66. https://doi.org/10.1016/j.lithos.2005.01.003.
Ward, N.D., Bianchi, T.S., Medeiros, P.M., Seidel, M., Richey, J.E., Keil, R.G., Sawakuchi, H.O., 2017. Where Carbon Goes When Water Flows: Carbon Cycling across the Aquatic Continuum. Front. Mar. Sci. 4 https://doi.org/10.3389/fmars.2017.00007.
Weiler, R.R., Chawla, V.K., 1969. Dissolved mineral quality of the Great Lakes. In: 12th Conference Great Lake Research, pp. 801–818.
Wittmann, H., Oelze, M., Gaillardet, J., Garzanti, E., & von Blanckenburg, F. (2020). A global rate of denudation from cosmogenic nuclides in the Earth's largest rivers. Earth-Science Reviews, 204, 103147. https://doi.org/Doi: 10.1016/j.earscirev.2020.103147.
Wu, L., Huh, Y., Qin, J., Du, G., van Der Lee, S., 2005. Chemical weathering in the Upper Huang He (Yellow River) draining the eastern Qinghai-Tibet Plateau. Geochim. Cosmochim. Acta 69 (22), 5279–5294. https://doi.org/10.1016/j.gca.2005.07.001.
Wysocka, A., Swierczewska, A., 2003. Alluvial deposits from the strike-slip fault Lo River Basin (Oligocene/Miocene), Red River Fault Zone, north-western Vietnam. J. Asian Earth Sci. 21 (10), 1097–1112. https://doi.org/10.1016/s1367-9120(02)00171-2.
Xiao, W., Lee, X., Hu, Y., Liu, S., Wang, W., Wen, X., Werner, M., Xie, C., 2017. An Experimental Investigation of Kinetic Fractionation of Open-Water Evaporation Over a Large Lake. J. Geophys. Res. Atmos. 122 (21) https://doi.org/10.1002/2017jd026774.
Yang, Y.-Y., Xu, Y.-S., Shen, S.-L., Yuan, Y., Yin, Z.-Y., 2014. Mining-induced geo-hazards with environmental protection measures in Yunnan, China: an overview. Bull. Eng. Geol. Environ. 74 (1), 141–150. https://doi.org/10.1007/s10064-014-0608-6.